



Athanasiadou, GE., Nix, AR., & McGeehan, JP. (1996). *Indoor 3D ray tracing predictions and their comparison with high resolution wideband measurements*. 36 - 40. <https://doi.org/10.1109/VETEC.1996.503403>

Peer reviewed version

Link to published version (if available):
[10.1109/VETEC.1996.503403](https://doi.org/10.1109/VETEC.1996.503403)

[Link to publication record in Explore Bristol Research](#)
PDF-document

University of Bristol - Explore Bristol Research

General rights

This document is made available in accordance with publisher policies. Please cite only the published version using the reference above. Full terms of use are available:
<http://www.bristol.ac.uk/red/research-policy/pure/user-guides/ebr-terms/>

Indoor 3D Ray Tracing Predictions and their Comparison with High Resolution Wideband Measurements

G.E. Athanasiadou, A.R. Nix and J.P. McGeehan

Centre for Communications Research, University of Bristol
Queen's Building, University Walk, Bristol, BS8 1TR, UK
Fax: +44 (0)117 9255265, Tel: ++44 (0)117 9287740,
E-mail: G.Athanasiadou@bristol.ac.uk

Abstract: This paper investigates the viability of an 'image based' 3D indoor propagation algorithm for characterising the radio channel in both LOS and non-LOS locations. The channel characteristics were also studied for different receiver antenna orientations. Predictions from the model are compared with high resolution channel impulse response measurements. The measurements highlight the high degree of variability experienced in the indoor channel. The results illustrate that with sufficient detail in the ray model reasonable agreement can be obtained for the power delay profiles.

I. INTRODUCTION

As indoor communication systems continue to evolve the need for more efficient propagation models will increase. Due to the site-specific nature of the indoor environments, tools are required which take into account the location, the orientation and the electrical properties of individual walls and objects. In recent years, ray tracing has emerged as a viable technique for producing deterministic channel models based on the processing of user-defined environments. Such models can be used to obtain sets of results that may be impractical or too costly to obtain by measurements.

In this paper, predictions from an indoor propagation model are compared with a number of wideband complex impulse response measurements. The model uses an indoor three-dimensional ray tracing algorithm for single floor scenarios, capable of supporting objects such as doors, windows, partitions, work benches, metal cabinets as well as external building structures. The algorithm uses a hybrid imaging technique where the two-dimensional image generations on vertical and horizontal planes are combined to produce the three dimensional paths.

II. MODELLING APPROACH AND ASSUMPTIONS

Ray tracing represents electromagnetic waves as rays which are generated from the transmitter and launched in three dimensional space. There are many types of ray-tracing techniques reported in the literature [1-7]. In this model a technique based on the electromagnetic theory of images has been developed [8, 9]. The model is capable of supporting

three dimensional single floor scenarios. To allow three dimensional paths to be found, a vertical ray trace is performed based on the results of the horizontal analysis. The vertical ray tracing also works with image theory but without the diffraction effects. An example for a simple line-of-sight case is illustrated in figure 1. As shown in the figure, rays whose paths fall partially outside of the buildings can also be modelled.

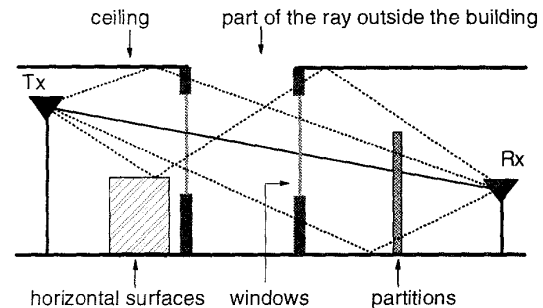


Figure 1: Ray tracing on the vertical plane.

The field calculation is implemented using three dimensional vector analysis with each ray considered separately. The model incorporates three dimensional antenna patterns for any antenna orientation. Each wall is characterised by its permittivity, conductivity and thickness. Wall thickness is required in the calculation of reflected and transmitted field strengths. The reflection, diffraction and transmission coefficients are evaluated as a function of the incident angle for a range of different wall materials.

In the building database all the walls are assumed to be perpendicular to the floor but not necessarily to each other. As can be seen in figure 1, the program has been extended to support the modelling of horizontal surfaces such as tables and benches. To make the algorithm as realistic as possible, walls with multiple windows and doors, and also partitions, i.e. walls with heights less than the ceiling, can be included in the data base. The model allows the width, height and position of each object to be defined.

To maintain flexibility, wall transmission and corner diffraction are fully supported even for onward propagating cases, i.e. each wall transmission or corner diffraction can

undergo subsequent diffractions, reflections and transmissions. Although for microcellular studies wall transmission is often ignored, for indoor studies transmission is an important propagation mechanism, particularly for non-line-of-sight (NLOS) locations [9]. For each path, the maximum number of ray permutations on the horizontal and vertical plane is user defined. The speed of the model is obviously a function of the number of objects in the building database and the number of reflections, transmissions and diffractions permitted in the ray engine.

III. COMPARISON WITH MEASUREMENTS

In order to evaluate the performance of the indoor model, simulation results were compared with channel impulse responses taken in a real environment. The measurements were performed in the MSc lab of the University of Bristol. The horizontal plane of the indoor environment is illustrated in figure 2 as it is represented within the model. The lab is on the ground floor and has windows overlooking the University Walk. Note that the area around the MSc lab has also been included in the database. To visualise the environment, figure 3 depicts a 3D view of the MSc lab as it is modelled for the simulation. The electrical properties and characteristics of the doors and windows are those of wood and glass respectively. The floor, the ceiling and the various internal and external walls, are based on different types of stone and brick.

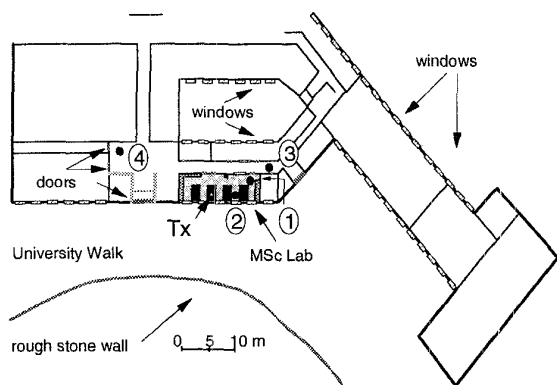


Figure 2: Ground plan of the environment under investigation.

Indoor propagation ray tracing models tend to assume empty rooms and do not include the effects of furniture. This is because the furniture locations and characteristics are often unknown or unavailable, and if considered they increase dramatically the complexity of the model. However, the contribution from the furniture may be very significant, especially if it includes metallic objects in close proximity to the antennas. Although it is impossible to fully describe an indoor environment, objects such as metallic cabinets are strong reflectors, and as such they should be included especially when they are close to the transmitter. Also,

particularly for the NLOS positions, the external or internal windows, through which the power propagates with far less loss than through walls, must be modelled. Finally, the signal characteristics will be different in an open area than an area filled with work benches.

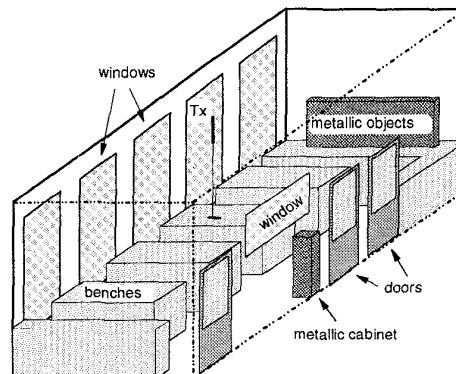


Figure 3: Three-dimensional representation of the environment.

The aim of the comparisons conducted in this paper was mainly to examine whether the ray tracing software could identify the major paths and their time delays and thus follow the trend of the measured power profiles. Since the limited time resolution of the measurements results in the vector addition of the rays with similar delays, in order to be able to distinguish the different rays arriving at the receiver from various paths, a high time resolution of 1.25ns was used (equivalent to a spatial resolution of 0.4 metres).

The measurements were taken with a network analyser (HP 8532A) at a central frequency of 1823MHz. For each point, 16 profiles were measured within an area of 1 square metre. The reason why so many profiles were measured for each point, is that the actual profile shape can change significantly over a distance of several centimetres because of the phase of the arriving rays [10]. The profiles were then processed in order to find a mean measured profile and its standard deviation at each time sample. With this process the effects of phasor addition and temporal variations are minimised and the site specific comparison becomes feasible. The transmitter was placed at a height of 3.6m at location 'Tx' in figure 2 and the receiving antenna height was 1.8m. The transmitted power was 10dBm. Standard dipole antennas were used for both the transmitter and the receiver.

Simulation results were obtained for up to 4 orders of reflection and 7 orders of wall transmission on the horizontal plane, while each ray could have up to 8 orders of reflection on the vertical plane. The impulse response obtained from the ray tracing model corresponds to measurements made with infinite bandwidth, i.e. each received ray is a perfect impulse in the time domain. To be able to compare simulated results with real measurements, the impulse response was

convolved with the network analyser’s filter. In a manner similar to the measurements, a grid analysis of 25 points (5 by 5) was performed over a 1 square metre area at each site, to calculate the averaged simulated profile. This profile was then compared with the mean and the standard deviation profiles of the measurements.

IV. RESULTS

Measurements were performed at four different sites. With the transmitter always vertically polarised, for each point two sets of measurements were taken: one with vertical and one with horizontal receiving dipoles. Two of the locations were in LOS and two in NLOS area of the transmitter.

The first point, point 1 in figure 2, is at the end of the lab, surrounded by work benches. As shown in figures 4 and 5, the simulated profile remains within the limits of the standard deviation of the measurements for the majority of the time. As expected, the predictions for the cross-polarisation cases proved to be a more difficult task. Since the dominant rays are weaker than in the vertical case, the scatterers become more important and the standard deviation of the measurements is higher. The second LOS measurement was close to the windows, at Point 2 in figure 2. For the co-polar case (figure 6), the simulation finds the dominant peaks of the measured profile and follows it for most of the time. The predicted profile for the horizontal dipole as shown in figure 7, was less accurate although still represents a reasonable match.

The first point under NLOS conditions was in the corridor, shown as point 3 in figure 2. Due to its position, rays can reach the area from a number of different paths. The measurements in all NLOS positions showed high standard deviation with respect to their mean profile. The mean simulated profile remains within the area of the measured standard deviation for the majority of time delays, and successfully predicts most of the peaks, although not always with the correct amplitude, (figure 8). In the case of the horizontal dipole major rays were not found, (figure 9). Generally for the NLOS positions, the prediction becomes more difficult not only because of the absence of dominant rays, but also because of the representation of the walls as homogeneous dielectric materials. Also as the distance between the receiver and the transmitter increases, the power profiles become more sensitive to the antenna orientation and a small change can have a serious impact on the results. The last measurement was at point 4 in figure 2, a location even further from the transmitter, at an open area at the entrance of the building. As can be seen from the predicted profiles in figures 10 and 11, the simulations remain within the standard deviation of the measurements, tracing most of the peaks. Note that when measured and simulated profiles show

poor agreement, there is a high deviation in the measured profile data.

In tables 1 and 2 below, the mean rms delay spread of both the measured and the simulated average profiles are shown. For the calculations a 30dB window relative to the peak of the profiles was used, except for the case of the horizontally polarised receiving dipole, for the NLOS case (points 3 and 4), where a 20dB window was used in order to stay above the noise floor of the measurements.

Point number	Measurements (ns)	Simulation (ns)
1	19.24	19.52
2	22.80	22.69
3	25.09	18.14
4	25.42	26.58

Table 1: Mean measured and simulated rms delay spread for the co-polar cases.

Point number	Measurements (ns)	Simulation (ns)
1	16.69	12.18
2	14.95	20.87
3	28.71	26.43
4	16.93	21.39

Table 2: Mean measured and simulated rms delay spread for the cross-polar cases.

From table1, it can be seen that for vertically polarised reception the predicted rms delay spread agrees remarkably well with those measured. Only point 3 (NLOS) shows any significant deviation, with the simulation underpredicting by approximately 7ns. The horizontally polarised data in table 2 shows slightly larger degrees of error, however the predictions still follow the trends successfully.

V. CONCLUSIONS

This paper has shown the viability of an ‘image based’ 3D indoor propagation model for characterising the radio channel in both LOS and non-LOS locations. The results have illustrated that with sufficient detail in the ray model reasonable agreement can be obtained for both co-polar and cross-polar power delay profiles. The measurements have highlighted the high degree of variability experienced in the indoor channel.

It can be concluded that although high accuracy in the simulated impulse responses can be difficult to achieve, the model can provide very good predictions for the statistics of the radio channel. From a systems perspective, the results would allow the quality of service to be determined, a vital factor in the planning of future indoor systems.

ACKNOWLEDGEMENTS

G.E. Athanasiadou wishes to thank BNR Europe Ltd. for their financial support of this work. The authors would also like to acknowledge the support of their colleagues in the Centre for Communications Research and in particular Mark Beach and Krysia Sroka for their valuable help with the measurements.

REFERENCES

- [1] J.W. McKnown and R.L.Hamilton, "Ray-tracing as a design tool for radio networks", *IEEE Networks Mag.*, pp. 21-26, Nov. 1991.
- [2] M.C. Lawton, J.P. McGeehan, "The application of a deterministic ray launching algorithm for the prediction of radio channel characteristics in small-cell environments", *IEEE Trans. on Veh. Technol.*, vol. 43, no. 4, pp. 955-969, Nov. 1994.
- [3] S.Y. Seidel, T.S. Rappaport, "Site specific propagation prediction for wireless in-building personal communication system design", *IEEE Trans. Veh. Technol.*, vol. 43, no 4, pp. 879-891, November 1994.
- [4] W. Honcharenko, H.L. Bertoni, J.L. Dailing, J. Qian, H.D. Yee, "Mechanisms governing UHF propagation on single floors in modern office buildings", *IEEE Trans. Veh. Technol.*, vol. 41, no 4, pp. 496-504, November 1992.
- [5] K.J. Gladstone and J.P. McGeehan, "Computer simulation of multipath fading in the land mobile radio environment", *IEE Proc.*, vol. 27, Pt.G., pp.323-330, no. 6, Dec.1980.
- [6] R.A. Valenzuela, "A ray tracing approach to predicting indoor wireless transmission", *43rd IEEE VTC*, New Jersey, May 1993.
- [7] T.Kurner, D.J.Cichon, W.Wiesbeck, "Concepts and results of 3-D digital terrain-based wave propagation models: an overview", *IEEE J-SAC*, pp 1002-1012, Sept. 1993.
- [8] G.E. Athanasiadou, A.R. Nix, J.P McGeehan, "A new 3D Indoor Ray Tracing model with particular reference to predictions of power and RMS delay spread", *IEEE PIMRC 1995*, Toronto, Canada, September 1995, pp. 1161-1165.
- [9] G.E. Athanasiadou, A.R. Nix, J.P McGeehan, "An efficient 'imaged-based' propagation model for LOS and non-LOS applications", *IEE Colloquium on propagation in buildings, 1995/134*, June 1995.
- [10] G.E. Athanasiadou, A.R. Nix, J.P McGeehan, "A Ray Tracing Algorithm for Microcellular wideband propagation modelling", *45th IEEE VTC*, Chicago, USA, July 1995, pp. 261-265.

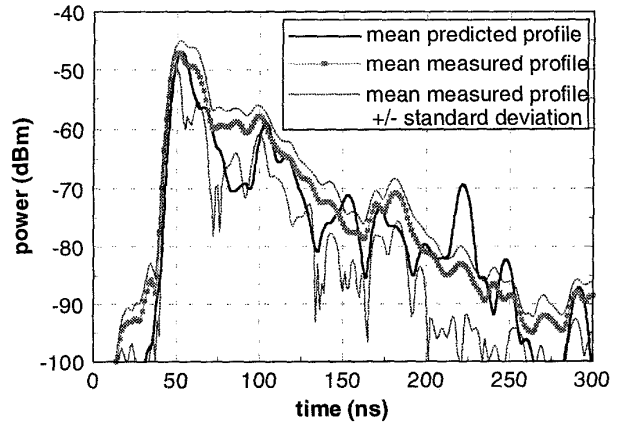


Figure 4: Point 1, Vertical dipole

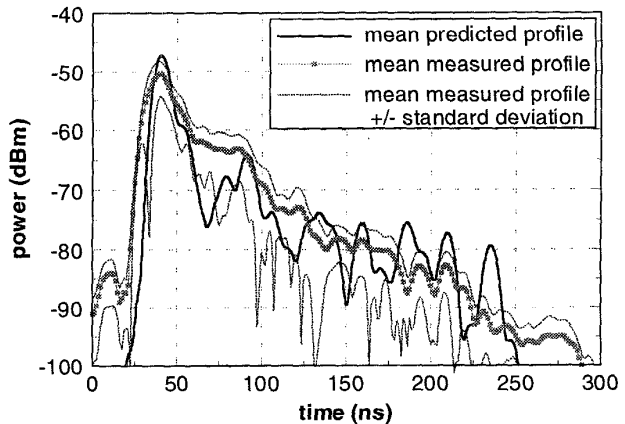


Figure 5: Point 1, Horizontal dipole

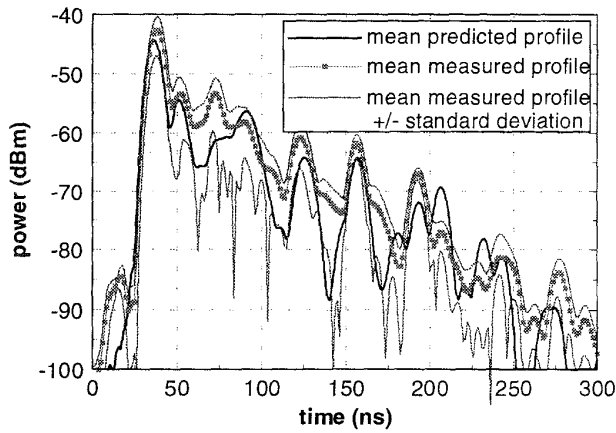


Figure 6: Point 2, Vertical dipole

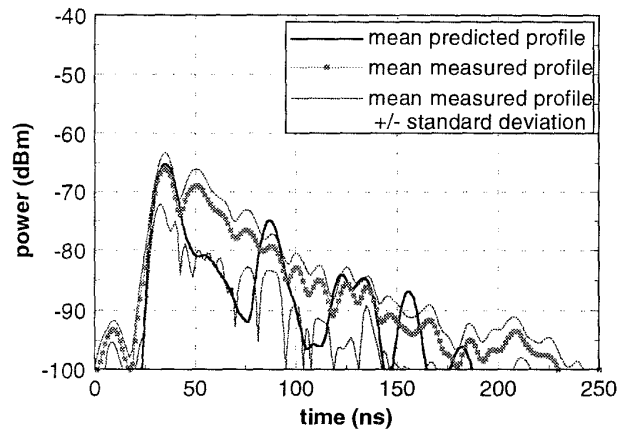


Figure 9: Point 3, Horizontal dipole

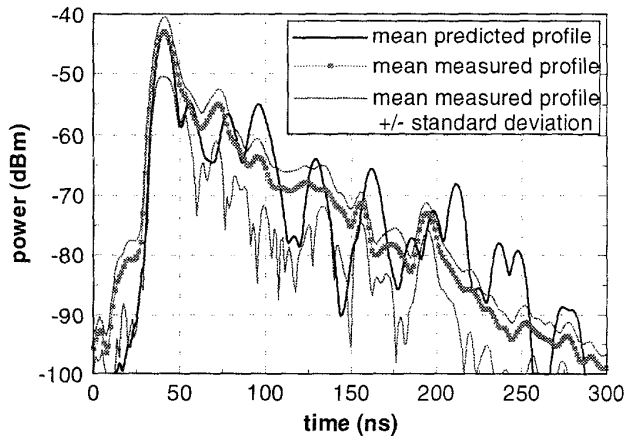


Figure 7: Point 2, Horizontal dipole

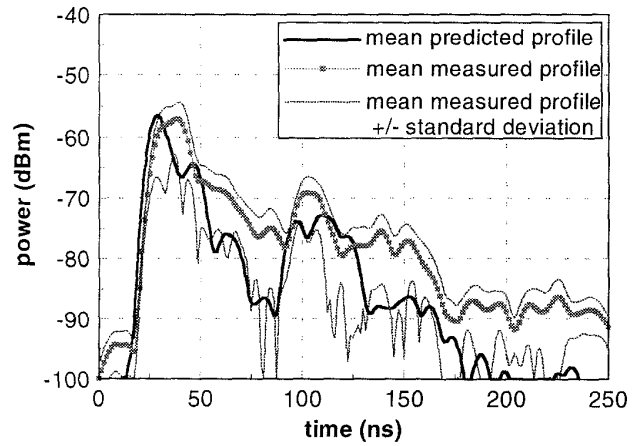


Figure 10: Point 4, Vertical dipole

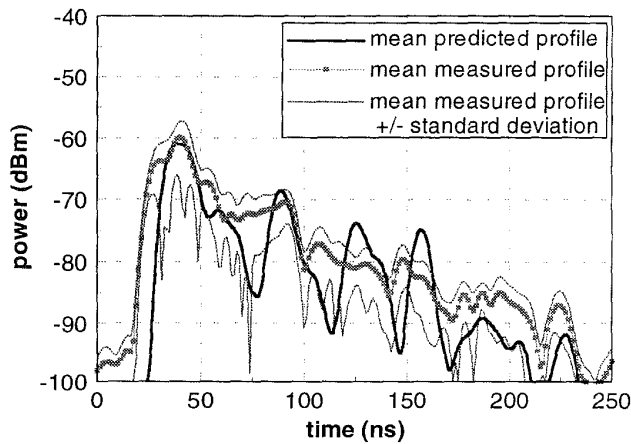


Figure 8: Point 3, Vertical dipole

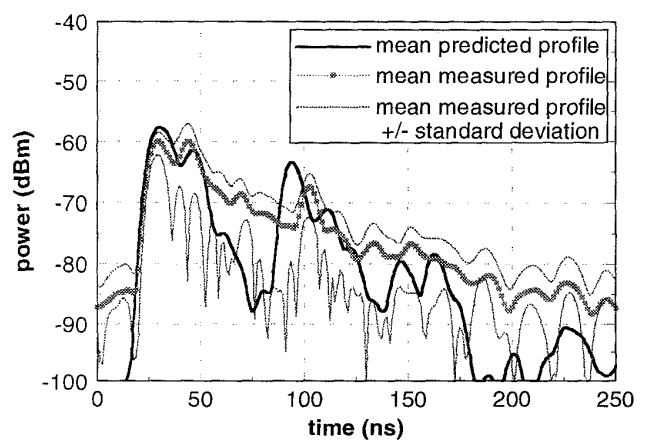


Figure 11: Point 4, Horizontal dipole